A new 30,000 year chronology for rapidly deposited sediments on the Lomonosov Ridge using bulk radiocarbon dating and probabilistic stratigraphic alignment

Francesco Muschitiello[1], Matt O'Regan[2], Jannik Martens[3], Gabriel West[2], Örjan Gustafsson[3], Martin Jakobsson[2]

[1] Department of Geography, University of Cambridge, Cambridge CB2 3EN, UK
[2] Department of Geological Sciences, Stockholm University, Svante Arrhenius väg 8, SE 106 91, Sweden
[3] Department of Environmental Science and Analytical Chemistry, Stockholm University, Svante Arrhenius väg 8, SE 106 91, Sweden

Correspondence to: Francesco Muschitiello (francesco.muschitiello@geog.cam.ac.uk)

Abstract. We present a new marine chronostratigraphy from a high-accumulation rate Arctic Ocean core at the intersection of the Lomonosov Ridge and the Siberian margin, spanning the last ~30 kyr. The chronology was derived using a combination of bulk ^{14}C dating and stratigraphic correlation to Greenland ice-core records. This was achieved by applying an appositely developed Markov chain Monte Carlo algorithm for Bayesian probabilistic alignment of proxy records. The algorithm simulates depositionally realistic alignments that are consistent with the available radiocarbon age estimates and allows deriving uncertainty bands associated with the inferred alignment. Current composite chronologies from this region are reasonably consistent with our age model during the Holocene and the latter part of deglaciation. However, prior to ~14 kyr BP they yield too old age estimates with offsets that linearly increase up to ~40 kyr near the onset of Marine Isotope Stage (MIS) 2. Our results challenge the robustness of previous regional chronostratigraphies and provide a new stratotype for correlation of sediment cores from this sector of the Lomonosov Ridge and East Siberian slope. In particular, they call for a re-interpretation of events in recent sea-ice proxy reconstructions (Xiao et al., 2015) inaccurately attributed to MIS-3 and the Last Glacial Maximum.

1 Introduction

Sedimentation rates along many of the Arctic margins are an order of magnitude higher (>5-10 cm/kyr) than in the central basins (<1-2 cm/kyr) (Wegner et al., 2015). These higher accumulation rates can provide detailed insights into glacial and Holocene Arctic paleoceanographic variability (i.e. (Jakobsson et al., 2010). High-resolution marine sediment cores from Arctic margins are used to constrain deglacial transgression of the shelves (Bauch et al., 2001; Cronin et al., 2017; Jakobsson et al., 2017; O'Regan et al., 2018), reconstruct variability in sea-ice (Stein and Fahl, 2000; De Vernal et al., 2005; Xiao et al., 2015), and fluxes of organic matter from rivers and coastal erosion (Hilton et al., 2015; Martens et al., 2019; Stein et al., 2001; Tesi et al., 2016).

Like all paleoclimate time series, Arctic Ocean reconstructions must be anchored in a robust chronology (Backman et al., 2004). Although tephra-chronology (Pearce et al., 2017) and paleosecular variation (Barletta et al., 2010; Lisé-Pronovost et al., 2009; Lund et al., 2016) were successfully applied in the Chukchi and Beaufort seas, radiocarbon dating of calcareous microfossils continues to underpin most Glacial and Holocene chronologies from the Arctic Ocean. However, the rare and often discontinuous occurrence of calcareous microfossils in Arctic Ocean sediments, commonly hinders the development of detailed age models. Altogether, these issues make the reconstruction of depositional histories of Arctic Ocean sedimentary records inherently challenging. One approach to overcome this is through stratigraphic correlation to independently dated sediment cores, or marker horizons (Alexanderson et al., 2014; O'Regan et al., 2019; Sellén et al., 2010). These regional composite stratigraphies provide a valuable tool for dating sediments, but can also result in perpetuating errors in the developed chronologies. As such there is a continued need to revisit, test and improve upon them, as well as to quantify age uncertainties to enable researchers to gauge interpretations and conclusions with respect to their results.

In this study we present a new detailed chronology of the last ~30 kyr for a core retrieved from an area with high sediment accumulation on the Asian end of the Lomonosov Ridge, bordering the east Siberian and Laptev Seas. The need for revising the chronology of sediments from this region of the Arctic emerged from discrepancies between a previously proposed age model and results from ^{14}C radiocarbon dating of bulk sediments.

The new chronology was derived by leveraging the temporal information from bulk radiocarbon dating and stratigraphic correlation to Greenland ice cores using a new probabilistic alignment algorithm appositely developed for this study. The benefits of the algorithm are threefold: it simulates depositionally realistic marine sediment-ice core proxy data alignments that are consistent with the existing independent radiocarbon age estimates; it ensures reproducibility of age-model solutions; it allows deriving age confidence bands inherent to the alignment process via Bayesian uncertainty inference. Our new age model results are considered in the context of published composite chronostratigraphies from this sector of the Arctic Ocean. Age discrepancies are quantified and implications of these findings are discussed.

2 Methods

2.1. Coring and study site

Core SWERUS-C3-31-PC (hereafter referred to as 31-PC) was acquired on Leg 2 of the SWERUS-C3 2014 Expedition on *IB Oden*, which departed August 21 from Barrow, Alaska, and ended October 3 in Tromsø, Norway. The core was retrieved from the intersection of the southern Lomonosov Ridge and the Siberian continental margin, bordering the East Siberian and Laptev seas (79.91˚ N; 143.23˚ E; 1120 m water depth) (Fig. 1). It was collected with a piston corer (PC) with an outside/inside diameter of 110/100 mm, rigged with a 1360-kg core head. The unsplit sediment cores were allowed to equilibrate to room temperature (20ºC) and subsequently logged shipboard on a Multi-Sensor Core Logger (MSCL). The cores were split and described shipboard, and imaged using a digital line-scanning camera.

2.2. Physical properties

Bulk density (ρ_B) and magnetic susceptibility (Bartington loop sensor) were measured at a downcore resolution of 1 cm on the MSCL (Fig. 2). Porosity (ϕ) was calculated from the MSCL measured bulk density using:

65
$$\phi = \frac{(\rho_G - \rho_B)}{(\rho_G - \rho_F)},\tag{1}$$

where a constant fluid density (ρ_F) of 1.024 g/cm^3 and grain density (ρ_G) of 2.67 ±0.01 g/cm^3 were applied. The grain density was determined by 11 shorebased measurements made on freeze-dried sediments from 31-PC using a Micromeritics, AccuPyc 1340, helium displacement pycnometer.

Sediment grain size (<2 mm) was measured at a 2 cm downcore resolution using a Malvern Mastersizer 3000 laser diffraction
70   particle size analyzer. Wet samples were immersed in a dispersing agent (<10% sodiumhexametaphosphate solution) and placed in an ultrasonic bath to ensure full particle disaggregation before analyses.

2.3. TOC analysis and ^{14}C dating

Bulk total organic carbon (TOC) analyses were performed after freeze-drying and homogenizing 80 samples taken from 31-PC at 10 cm intervals (Fig. 2). A split of ~10 mg of sediment was weighed in silver capsules and acidified with 3M HCl to
75   remove carbonates. The TOC of the samples was measured using a Carlo Erba NC2500 elemental analyzer in the Department of Geological Sciences, Stockholm University.

Eight bulk sediment samples and one marine mollusk shell were sent to NOSAMS for ^{14}C dating (Table 1). Despite shipboard and shore-based efforts, no further carbonate microfossils were found in 31-PC that could be used for radiocarbon dating. In order to remove carbonates from the bulk sediment samples, the samples received HCl vapor treatment. Results were reported
80   as conventional ^{14}C years (Stuiver et al., 1977) and then converted into ^{14}C calendar years (cal ka BP) using Calib 7.1 (Stuiver et al., 2018). Bulk ^{14}C estimates were calibrated using the IntCal13 radiocarbon calibration curve (Reimer et al., 2013), whereas the mollusk shell ^{14}C estimate was calibrated against Marine13 using $\Delta R = 0^{+1000}_{-400}$ to conservatively account for unknown changes in the local marine reservoir correction.

2.4. Chronology

85   ### 2.4.1 Probabilistic algorithm for stratigraphic alignment

In the absence of independent means for constraining the chronology of core 31-PC and due to the scarce fossiliferous content, we here rely on a novel combination of *i*) bulk radiocarbon dating and *ii*) proxy-to-proxy stratigraphic alignment. Both dating strategies come with limitations and benefits. For instance, bulk sediment dates do not always reflect the true depositional age

of the associated stratum and can yield considerably older ages due to varying contamination with ^{14}C-dead carbon. However, despite its inherent poor accuracy, bulk dating still offers valuable chronological information as it generally provides a maximum estimate of the age of deposition for a particular stratum. On the other hand, correlation of proxy-climate records leans on the assumption that changes in a particular stratigraphic parameter in an undated record correspond to approximately contemporaneous events in a master reference record that contains direct dating information. This method, though theoretically accurate, always has potential for subjectivity. As such, manual identification of tie points across the input and target records introduces subjective constraints on sedimentation rate changes, which are often difficult to validate and do not incorporate uncertainties associated with the proposed alignment.

To surmount these issues and ultimately derive a chronology for 31-PC that leverages the strengths of both dating strategies, we applied a tailor-made hidden Markov model alignment algorithm. The algorithm evaluates alignments probabilistically based on direct observations of sedimentation rate changes from radiocarbon data measured on the sediment core of interest. This strategy not only improves alignment accuracy, but produces realistic alignments, ensures reproducibility, and allows deriving Bayesian credible bands associated with the alignment procedure.

In our algorithm, radiocarbon dates are used as gateways to bound a relatively large empirical and depositionally-realistic depth-age space that conservatively encapsulates the sedimentation history of the record of interest. This domain is subsequently explored by sampling alignments between an input proxy record and an independently-dated target record in proportion to their probability. More explicitly, in this study we use observed sedimentation rate changes, inferred from the available bulk (and one fossiliferous) ^{14}C estimates (Table 1), to probabilistically evaluate the alignments between sediment porosity (ϕ) from 31-PC –a robust sedimentological parameter mainly reflecting grain size variations– and GISP2 δ^{18}O data (Seierstad et al., 2014) –an indicator of large-scale climate variability. The alignment hinges on the assumption that shifts in sedimentological properties at our coring site and high-latitude climate, as recorded in Greenland ice cores, are virtually synchronous. This assumption is consistent with existing Arctic paleoceanographic reconstructions of the last glacial cycle, which show a good agreement with Greenland ice-core δ^{18}O profiles (Cronin et al., 2012). While considering the probabilities for sedimentation rate changes at our coring site, the algorithm estimates a sample of optimal alignments that relate the depth scale of 31-PC to the timescale underlying the GISP2 δ^{18}O data, i.e. the Greenland Ice Core Chronology 2005 (GICC05) (Rasmussen et al., 2006).

Our numerical approach builds upon previous work using Bayesian Markov chain Monte Carlo inversion for probabilistic alignment of paleoclimate records (Malinverno, 2013; Muschitiello et al., 2015; West et al., 2019), which has been successfully applied on a variety of terrestrial and marine archives (Muschitiello et al., 2019; Sessford et al., 2019; Wohlfarth et al., 2017). It should be noted that our algorithm, though analogous in spirit to that devised by (Lin et al., 2014), is fundamentally different. The method by (Lin et al., 2014) weighs the probability of an alignment between a given input and a target record according to a distribution of sedimentation rate change obtained from a spatial network of radiocarbon-based estimates from low

latitudes. Our method instead, rather than relying on compilation-based observations, employs direct in-situ radiocarbon estimates of depositional variability.

2.4.2 Statistical method

Prior to alignment, the input ϕ and target GISP2 $\delta^{18}O$ timeseries were scaled between -1 and 1. The alignment is described by random variables A_i, that relate the depth of the ith data point in the input record ($i=1, 2,\ldots, n$) for all depths to unknown ages on the target GICC05 timescale. We then express an alignment vector $A=(A_1, A_2,\ldots, A_n)$ as a series of assignments of GICC05 ages for every depth in the input record $d=(d_1, d_2,\ldots, d_n)$ at which ϕ was measured. Note that this strategy circumvents the shortcomings of using interpolation to process unevenly spaced data and enables alignment of each individual ϕ data point to the GISP2 $\delta^{18}O$ record. The alignment vector is defined at any point i on the depth scale of 31-PC by a linear interpolation between 11 depth-age nodes (Fig. 3 and Table 1): one surface node; one node based on a mollusk shell ^{14}C estimate; eight nodes based on bulk ^{14}C estimates; and one perturbed node at a random location d_k ($k=2, 3,\ldots, n-1$) to ensure sampling sedimentation rate changes between any two consecutive empirical age constraints. The nodes strictly follow depth-age paths that do not violate the principle of superposition in order to ensure that the depositional age of the input record increases monotonically with depth. Considering a perturbed node at depth d_k, sedimentation rates between two adjacent levels d_k and $d_{k\pm1}$ are allowed to change over a wide range of values spanning ~0.01-100 cm/yr.

Since the alignment process is fundamentally uncertain, we apply probability theory in the age assignments of the alignment vector A. Specifically, the requirement of a good match between the ϕ and the GISP $\delta^{18}O$ records that at the same time accounts for unobserved changes in sedimentation rates is here derived using Bayes' rule of probabilistic inference. The rule combines the probability that the given ϕ data would be observed for a particular alignment (i.e. the likelihood model), with the probability that a given alignment would be observed independent of any ϕ data (i.e. the prior model).

The likelihood is specified by the probability for a given residual misfit between the aligned ϕ record and the target GISP2 $\delta^{18}O$. In the alignment problem posed here, it determines the set of nodes that give a good alignment between the input and the target by weighing the competing needs of a small root-mean-square deviation ($RMSE$) and a high coefficient of correlation (r). The $RMSE$ formula is:

$$RMSE = \sqrt{\frac{1}{N}\sum_{i=1}^{N}(P_i - O_i)^2} \, , \tag{2}$$

where N is the number of aligned data points in the input record, O_i is the rescaled ϕ value for i^{th} point in the input record, and P_i is the corresponding rescaled GISP2 $\delta^{18}O$ value of a proposed alignment.

The prior, on the other hand, is specified by the probability of any given depth-age function. The posterior probability for any given alignment is proportional to the product of likelihood and prior, and can be written as follows:

150 $$P(A_j|data, \varphi, \theta) = \frac{P(data|A_j, \theta)\, P(A_j|\varphi)}{\sum_{i=1}^{k} P(data|A_i, \theta)\, P(A_i|\varphi)} \qquad j = 1, 2, \ldots, k \qquad\qquad (3)$$

where φ are the parameters associated with the alignment and θ the parameters used in the likelihood model. The denominator in equation (3) reflects the full likelihood calculated by summing over all possible k mutually exclusive and exhaustive alignments.

The notation $P(data|A, \theta)$ gives the probability that the input ϕ record would be observed for a particular alignment A. The
155 notation $P(A|\varphi)$ specifies the probability for the alignment vector A given the parameters used to constrain the depth-age model relationship (i.e. the depth-age nodes). $P(A|data, \varphi, \theta)$ gives the posterior probability of a given alignment. Calculation of the posterior probability proceeds by sampling an initial value for each unknown parameter from the associated prior distributions using a reversible jump Markov chain Monte Carlo (MCMC) sampling (Vihola, 2012). The algorithm continues by:

160 1. Proposing a "candidate" depth-age model and the resulting alignment between the input ϕ data and the target GISP2 δ^{18}O record.

2. Accepting or rejecting the candidate depth-age model (and associated alignment) according to its posterior probability using the Metropolis-Hasting algorithm (Hastings, 1970; Metropolis et al., 1953), whereby the posterior probability is higher for alignment functions that yield a closer match between ϕ and GISP2 δ^{18}O (i.e. as defined by a relatively smaller *RMSE* and
165 higher *r*).

3. Repeat from step 1 for 5 x 10^5 iterations.

By convention the sample was divided in two parts. We discarded the initial 10^5 samples ("burn in" period), which in our case corresponds to the MCMC sample length necessary to reach model convergence. The median of the remainder alignment sample was used to infer the posterior optimal correlation while its variability was used to obtain posterior alignment credible
170 bands. Similarly, the sample of accepted depth-age models was used to find posterior median and credible bands for the chronology of 31-PC.

3. Results and discussion

3.1 Evaluating the existing regional chronology

175 Sediment physical property measurements (bulk density, magnetic susceptibility, grain size and TOC) performed on 31-PC allow us to firmly establish a lithostratigraphic correlation to a neighboring sediment core (PS2767-4) collected by *RV Polarstern* during Expedition ARK-XI/1 in 1995 (Rachor, 1997). PS2767-4 is underpinned by a published composite

chronology that was constructed using cross-correlation and the amalgamation of dating information across a number of regional marine sediment sequences (Figs. 1 and 2) (Stein et al., 2001; 2012).

Core PS2767-4 is located only 24 km south of 31-PC (Fig. 1). This 8.22 m long core is thought to be younger than 60 kyr BP, implying that it contains a complete record of MIS-3 through 1 (Stein et al., 2001; 2012). It has been used to investigate organic matter delivery from the Laptev shelf (Stein et al., 2001; Stein and Fahl, 2000), and more recently for biomarker based reconstructions of sea ice variability during the last glacial cycle (Stein et al., 2012; Xiao et al., 2015).

The Holocene and postglacial age model for PS2767-4 was dated primarily using ^{14}C radiocarbon dates on three mollusk shells, while the pre-Holocene stratigraphy is based on correlation to other records where oxygen isotopes, magnetostratigraphy and dinoflagellate biostratigraphy have been used to infer approximate ages (Stein et al., 2001). These older regional age constraints were mapped onto PS2767-4 using a regional correlation between magnetic susceptibility records and sediment lithology (Stein et al., 2001). Stein and Fahl (2012) recognized that in the absence of direct dating, the pre-Holocene stratigraphy of this record remained tentative. (Figs. 1 and 2). Examination of the stratigraphic profiles for 31-PC and PS-2767-4 on their independent depth scale reveals an unequivocal coherence across multiple parameters, which argues in favor of a consistent depositional history at the two sites (Fig. 2).

Although the postglacial and Holocene age model for PS-2767-4 is fairly robust, being variably dated by ^{14}C measurements in each of the correlated records, the inferred ages for glacial sediments (MIS 2-4) are considerably less well-constrained (Fig. 2) (Stein et al., 2012). Boundaries between MIS 2, 3, and 4 are demarcated mainly by correlative changes in sediment lithology, organic matter content and dated using a dinocyst-based stratigraphy developed for PS2471-1 (Matthiessen et al., 2001) (Fig. 1). Results from our bulk ^{14}C radiocarbon dates illustrate a clear deviation in the proposed age model for PS-2767-4 beyond ~14 kyr BP. The two near-bottom bulk ^{14}C dates yield an uppermost bound of ~31.8 and ~33.5 kyr BP (Table 1, Fig. 2) for the base of 31-PC. Given that the near-basal depositional age of 31-PC cannot be older than the late MIS-3/early MIS-2, it seems unlikely that sediment from PS2767-4 can date back to 60 kyr BP (i.e. MIS-4), as previously suggested (Stein et al., 2012).

3.2 Proposed age model

The outcomes of the probabilistic alignment and the resulting age model for 31-PC are presented in Figure 3. The correlation between ϕ and GISP2 δ^{18}O requires some considerations. Large-scale climate shifts may not be manifested in a similar way in different proxies. In fact, our ϕ record integrates a number of processes, such as sediment grain size, composition, transport and deposition at the coring site. By contrast, GISP δ^{18}O is responsive to changes in Greenland air temperature. Therefore, the two parameters likely do not scale in a linear fashion, and a perfect match should not be expected. Nonetheless, the degree of correlation between the marine and ice-core data –especially during deglaciation and MIS-2– is surprisingly well defined and overall compelling.

The results show that 31-PC features relatively linear sedimentation rates with a mean of ~41 ±24 (1σ) cm/kyr, with the exception of the last ~9 kyr where sedimentation rates are slightly lower (~15 cm/kyr) (Fig. 3). This is in line with the expected decrease in depositional rate resulting from post-glacial transgression of the Siberian shelves (Bauch et al., 2001; Tesi et al., 2016).

The mean 99% posterior credible intervals for our age model is ~±1.46 kyr (Fig. 3). Mean uncertainties are larger during the Holocene (~±1.85 kyr). The larger age error, reflects on one hand the absence of radiocarbon-based age constraints in the upper 1.4 m, and on the other hand the lack of structure in the ϕ and GISP2 δ^{18}O data during the Holocene, which makes the match statistically less robust (Fig. 3).

3.3 Implications of the new age model

The implications of these findings are critical for reconstructing and understanding the oceanographic history in this region of the Arctic Ocean. The revised age model reveals substantially faster sedimentation rates during the LGM and deglaciation, compared to the existing regional chronology (Fig. 4). Published proxy reconstructions based on the original chronology of PS2767-4, and putatively assigned to the Last Glacial Maximum (LGM)/MIS-2 and MIS-3, are flawed. Hence, the reconstructed paleoceanographic timeline before deglaciation and related interpretations may not be fully reliable and should be taken with caution. In particular, the attribution of events in recent low-resolution biomarker-based reconstructions of Arctic sea ice conditions (Xiao et al., 2015) require revision for this sector of the Arctic Ocean. This is important, as currently PS2767-4 is the only record from the currently seasonally ice covered southern Lomonosov Ridge where glacial and deglacial reconstructions of sea ice exist (Fig. 4). We suggest that the sea-ice record should be interpreted differently than as outlined in the original publication. According to the new marine chronology presented in this study, variable –though generally more extensive than present day– sea-ice cover characterized the central Arctic Ocean during the early LGM/MIS-2 (rather than during the latter part of MIS-3); the second half of deglaciation (rather than LGM/MIS-2) featured increasing sea-ice growth with permanent sea ice throughout the year; decreased sea-ice cover occurred around the transition between deglaciation and the Holocene (rather than during deglaciation) (Fig. 4).

4. Conclusions

We present a new chronostratigraphy from the Asian end of the Lomonosov Ridge spanning the last ~30 kyr using a combination of bulk radiocarbon dating and stratigraphic correlation to Greenland ice-core records. The alignment was obtained using a novel probabilistic stratigraphic alignment algorithm. The algorithm simulates correlations of marine and ice-core proxy records that are consistent with the observed changes in sedimentation rates obtained from independent radiocarbon dates, and ultimately yields uncertainty bands associated with the alignment process.

Stratigraphic comparison with a nearby record constrained by a composite regional age model highlights substantial chronological shortcomings in this region prior to ~14 kyr BP. We identified a linearly increasing age offset that builds up to ~40 kyr at the beginning of LGM/MIS-2 and that question previous attributions of plaeoceanographic events from MIS-3 to the early deglaciation. Specifically, our results allowed us to partly re-interpret the sequence of events observed in a recent sea-ice proxy reconstruction from the central Arctic Ocean (Xiao et al., 2015).

Our new chronostratigraphy constitutes an important regional benchmark that helps revise the paleoceanographic timeline of the central Arctic from MIS-2 to 1, and can serve as a template for future correlations of regional sediment sequences with poor independent age control.

Author contribution: FM and MO initiated the study and wrote the manuscript. FM designed the Bayesian probabilistic alignment method and constructed the chronology of core SWERUS-C3-31-PC. JM performed the TOC analysis and did the sampling for ^{14}C dating. GW performed the physical properties analyses with assistance from MO. OG and MJ participated with the interpretation of the results. All authors were involved in editing the manuscript.

Data availability: The source data underlying Figure 2 (porosity, bulk density, grain size, magnetic susceptibility and total organic carbon content) and Figure 3 (age model and inferred uncertainties) are provided as Supplementary Data files with the online version of this article on the publisher's website and via the Bert Bolin Centre for Climate Research database (https://bolin.su.se/data/XXXXXX).

Competing interests: The authors declare that they have no conflict of interest.

Acknowledgements

We thank the supporting crew and Captain of I/B Oden and the support of the Swedish Polar Research Secretariat during the SWERUS-C3 expedition. This research and the expedition were supported by the Knut and Alice Wallenberg Foundation (KAW) and by Swedish Research Council awards to MO, MJ and OG.

References

Alexanderson, H., Backman, J., Cronin, T. M., Funder, S., Ingolfsson, O., Jakobsson, M., Landvik, J. Y., Löwemark, L., Mangerud, J. and März, C.: An Arctic perspective on dating Mid-Late Pleistocene environmental history, Quat. Sci. Rev., 92, 9–31, 2014.

Backman, J., Jakobsson, M., Løvlie, R., Polyak, L. and Febo, L. A.: Is the central Arctic Ocean a sediment starved basin?, Quat. Sci. Rev., 23(11–13), 1435–1454, 2004.

265 Barletta, F., St-Onge, G., Channell, J. E. T. and Rochon, A.: Dating of Holocene western Canadian Arctic sediments by matching paleomagnetic secular variation to a geomagnetic field model, Quat. Sci. Rev., 29(17–18), 2315–2324, 2010.

Bauch, H. A., Mueller-Lupp, T., Taldenkova, E., Spielhagen, R. F., Kassens, H., Grootes, P. M., Thiede, J., Heinemeier, J. and Petryashov, V. V: Chronology of the Holocene transgression at the North Siberian margin, Glob. Planet. Change, 31(1–4), 125–139, 2001.

270 Cronin, T. M., Dwyer, G. S., Farmer, J., Bauch, H. A., Spielhagen, R. F., Jakobsson, M., Nilsson, J., Briggs Jr, W. M. and Stepanova, A.: Deep Arctic Ocean warming during the last glacial cycle, Nat. Geosci., 5(9), 631, 2012.

Cronin, T. M., O'Regan, M., Pearce, C., Gemery, L., Toomey, M., Semiletov, I. and Jakobsson, M.: Deglacial sea level history of the East Siberian Sea and Chukchi Sea margins, Clim. Past, 13(9), 1097, 2017.

Fahl, K. and Stein, R.: Modern seasonal variability and deglacial/Holocene change of central Arctic Ocean sea-ice cover: new 275 insights from biomarker proxy records, Earth Planet. Sci. Lett., 351, 123–133, 2012.

Hastings, W. K.: Monte carlo sampling methods using Markov chains and their applications, Biometrika, doi:10.1093/biomet/57.1.97, 1970.

Hilton, R. G., Galy, V., Gaillardet, J., Dellinger, M., Bryant, C., O'Regan, M., Gröcke, D. R., Coxall, H., Bouchez, J. and Calmels, D.: Erosion of organic carbon in the Arctic as a geological carbon dioxide sink, Nature, 524(7563), 84, 2015.

280 Jakobsson, M., Long, A., Ingólfsson, Ó., Kjær, K. H. and Spielhagen, R. F.: New insights on Arctic Quaternary climate variability from palaeo-records and numerical modelling, Quat. Sci. Rev., 29(25–26), 3349–3358, 2010.

Jakobsson, M., Pearce, C., Cronin, T. M., Backman, J., Anderson, L. G., Barrientos, N., Björk, G., Coxall, H., De Boer, A. and Mayer, L. A.: Post-glacial flooding of the Bering Land Bridge dated to 11 cal ka BP based on new geophysical and sediment records, Clim. Past, 13(8), 991, 2017.

285 Lin, L., Khider, D., Lisiecki, L. E. and Lawrence, C. E.: Probabilistic sequence alignment of stratigraphic records, Paleoceanography, doi:10.1002/2014PA002713, 2014.

Lisé-Pronovost, A., St-Onge, G., Brachfeld, S., Barletta, F. and Darby, D.: Paleomagnetic constraints on the Holocene stratigraphy of the Arctic Alaskan margin, Glob. Planet. Change, 68(1–2), 85–99, 2009.

Lisiecki, L. E. and Raymo, M. E.: A Pliocene-Pleistocene stack of 57 globally distributed benthic δ18O records, 290 Paleoceanography, 20(1), 2005.

Lund, S., Keigwin, L. and Darby, D.: Character of Holocene paleomagnetic secular variation in the tangent cylinder: evidence

from the Chukchi Sea, Phys. Earth Planet. Inter., 256, 49–58, 2016.

Malinverno, A.: Data report: Monte Carlo correlation of sediment records from core and downhole log measurements at Sites U1337 and U1338 (IODP Expedition 321)., 2013.

295   Martens, J., Wild, B., Pearce, C., Tesi, T., Andersson, A., Bröder, L., O'Regan, M., Jakobsson, M., Sköld, M. and Gemery, L.: Remobilization of old permafrost carbon to Chukchi Sea sediments during the end of the last deglaciation, Global Biogeochem. Cycles, 33(1), 2–14, 2019.

Matthiessen, J., Knies, J., Nowaczyk, N. R. and Stein, R.: Late Quaternary dinoflagellate cyst stratigraphy at the Eurasian continental margin, Arctic Ocean: indications for Atlantic water inflow in the past 150,000 years, Glob. Planet. Change, 31(1–300   4), 65–86, 2001.

Metropolis, N., Rosenbluth, A. W., Rosenbluth, M. N., Teller, A. H. and Teller, E.: Equation of state calculations by fast computing machines, J. Chem. Phys., doi:10.1063/1.1699114, 1953.

Müller, C. and Stein, R.: Variability of fluvial sediment supply to the Laptev Sea continental margin during Late Weichselian to Holocene times: Implications from clay-mineral records, Int. J. Earth Sci., 89(3), 592–604, doi:10.1007/s005310000112, 305   2000.

Muschitiello, F., Pausata, F. S. R., Watson, J. E., Smittenberg, R. H., Salih, A. A. M., Brooks, S. J., Whitehouse, N. J., Karlatou-Charalampopoulou, A. and Wohlfarth, B.: Fennoscandian freshwater control on Greenland hydroclimate shifts at the onset of the Younger Dryas, Nat. Commun., 6, 8939, doi:10.1038/ncomms9939, 2015.

Muschitiello, F., D'Andrea, W. J., Schmittner, A., Heaton, T. J., Balascio, N. L., deRoberts, N., Caffee, M. W., Woodruff, T. 310   E., Welten, K. C., Skinner, L. C., Simon, M. H. and Dokken, T. M.: Deep-water circulation changes lead North Atlantic climate during deglaciation, Nat. Commun., doi:10.1038/s41467-019-09237-3, 2019.

O'Regan, M., Coxall, H., Hill, P., Hilton, R., Muschitiello, F. and Swärd, H.: Early Holocene sea level in the Canadian Beaufort Sea constrained by radiocarbon dates from a deep borehole in the Mackenzie Trough, Arctic Canada, Boreas, 47(4), 1102–1117, 2018.

315   O'Regan, M., Coxall, H. K., Cronin, T. M., Gyllencreutz, R., Jakobsson, M., Kaboth, S., Löwemark, L., Wiers, S. and West, G.: Stratigraphic Occurrences of Sub-Polar Planktonic Foraminifera in Pleistocene Sediments on the Lomonosov Ridge, Arctic Ocean, Front. Earth Sci., 7, 71, 2019.

Pearce, C., Varhelyi, A., Wastegård, S., Muschitiello, F., Barrientos, N., O'Regan, M., Cronin, T. M., Gemery, L., Semiletov, I. and Backman, J.: The 3.6 ka Aniakchak tephra in the Arctic Ocean: a constraint on the Holocene radiocarbon reservoir age 320   in the Chukchi Sea, Clim. Past, 13(4), 303, 2017.

Rachor, E.: Scientific cruise report of the Arctic expedition ARK-XI/1 of RV" Polarstern" in 1995, Reports Polar Res. Alfred

Wegener Inst. Polar Mar. Res. Bremerhaven, 226, 1997.

Rasmussen, S. O., Andersen, K. K., Svensson, A. M., Steffensen, J. P., Vinther, B. M., Clausen, H. B., Siggaard-Andersen, M. L., Johnsen, S. J., Larsen, L. B., Dahl-Jensen, D., Bigler, M., Röthlisberger, R., Fischer, H., Goto-Azuma, K., Hansson, M. E. and Ruth, U.: A new Greenland ice core chronology for the last glacial termination, J. Geophys. Res. Atmos., 111(6), doi:10.1029/2005JD006079, 2006.

Reimer, P. J., Bard, E., Bayliss, A., Beck, J. W., Blackwell, P. G., Bronk Ramsey, C., Buck, C. E., Cheng, H., Edwards, R. L., Friedrich, M., Grootes, P. M., Guilderson, T. P., Haflidason, H., Hajdas, I., Hatté, C., Heaton, T. J., Hoffmann, D. L., Hogg, A. G., Hughen, K. A., Kaiser, K. F., Kromer, B., Manning, S. W., Niu, M., Reimer, R. W., Richards, D. A., Scott, E. M., Southon, J. R., Staff, R. A., Turney, C. S. M. and van der Plicht, J.: IntCal13 and Marine13 Radiocarbon Age Calibration Curves 0–50,000 Years cal BP, Radiocarbon, 55(4), 1869–1887, doi:10.2458/azu_js_rc.55.16947, 2013.

Seierstad, I. K., Abbott, P. M., Bigler, M., Blunier, T., Bourne, A. J., Brook, E., Buchardt, S. L., Buizert, C., Clausen, H. B., Cook, E., Dahl-Jensen, D., Davies, S. M., Guillevic, M., Johnsen, S. J., Pedersen, D. S., Popp, T. J., Rasmussen, S. O., Severinghaus, J. P., Svensson, A. and Vinther, B. M.: Consistently dated records from the Greenland GRIP, GISP2 and NGRIP ice cores for the past 104ka reveal regional millennial-scale δ18O gradients with possible Heinrich event imprint, Quat. Sci. Rev., doi:10.1016/j.quascirev.2014.10.032, 2014.

Sellén, E., O'Regan, M. and Jakobsson, M.: Spatial and temporal Arctic Ocean depositional regimes: a key to the evolution of ice drift and current patterns, Quat. Sci. Rev., 29(25–26), 3644–3664, 2010.

Sessford, E. G., Jensen, M. F., Tisserand, A. A., Muschitiello, F., Dokken, T., Nisancioglu, K. H. and Jansen, E.: Consistent fluctuations in intermediate water temperature off the coast of Greenland and Norway during Dansgaard-Oeschger events, Quat. Sci. Rev., 223, 105887, 2019.

Stein, R. and Fahl, K.: Holocene accumulation of organic carbon at the Laptev Sea continental margin (Arctic Ocean): Sources, pathways, and sinks, Geo-Marine Lett., 20, 27–36, doi:10.1007/s003670000028, 2000.

Stein, R., Boucsein, B., Fahl, K., Garcia de Oteyza, T., Knies, J. and Niessen, F.: Accumulation of particulate organic carbon at the Eurasian continental margin during late Quaternary times: Controlling mechanisms and paleoenvironmental significance, Glob. Planet. Change, 31, 87–104, doi:10.1016/S0921-8181(01)00114-X, 2001.

Stein, R., Fahl, K. and Müller, J.: Proxy reconstruction of Cenozoic Arctic Ocean sea ice history–from IRD to IP25, Polarforschung, 82(1), 37–71, 2012.

Stuiver, M., Polach, H. A., GODWIN, H., Stuiver, M. and Robinson, S. W.: Discussion Reporting of 14C Data, Radiocarbon, 19(03), 355–363, doi:10.1017/S0033822200003672, 1977.

Stuiver, M., Reimer, P. J. and Reimer, R. W.: CALIB 14C Calibration Program, 2018.

Tesi, T., Muschitiello, F., Smittenberg, R. H., Jakobsson, M., Vonk, J. E., Hill, P., Andersson, A., Kirchner, N., Noormets, R., Dudarev, O., Semiletov, I. and Gustafsson: Massive remobilization of permafrost carbon during post-glacial warming, Nat. Commun., doi:10.1038/ncomms13653, 2016.

355 De Vernal, A., Hillaire-Marcel, C. and Darby, D. A.: Variability of sea ice cover in the Chukchi Sea (western Arctic Ocean) during the Holocene, Paleoceanography, 20(4), 2005.

Vihola, M.: Robust adaptive Metropolis algorithm with coerced acceptance rate, Stat. Comput., doi:10.1007/s11222-011-9269-5, 2012.

Wegner, C., Bennett, K. E., de Vernal, A., Forwick, M., Fritz, M., Heikkilä, M., Łącka, M., Lantuit, H., Laska, M., Moskalik, 360 M., O'Regan, M., Pawłowska, J., Promińska, A., Rachold, V., Vonk, J. E. and Werner, K.: Variability in transport of terrigenous material on the shelves and the deep Arctic Ocean during the Holocene, Polar Res., doi:10.3402/polar.v34.24964, 2015.

West, G., Kaufman, D. S., Muschitiello, F., Forwick, M., Matthiessen, J., Wollenburg, J. and O'Regan, M.: Amino acid racemization in Quaternary foraminifera from the Yermak Plateau, Geochronol. Discuss., 2019, 1–26, doi:10.5194/gchron-365 2019-5, 2019.

Wohlfarth, B., Muschitiello, F., L. Greenwood, S., Andersson, A., Kylander, M., Smittenberg, R. H., Steinthorsdottir, M., Watson, J. and Whitehouse, N. J.: Hässeldala – a key site for Last Termination climate events in northern Europe, Boreas, doi:10.1111/bor.12207, 2017.

Xiao, X., Stein, R. and Fahl, K.: MIS 3 to MIS 1 temporal and LGM spatial variability in Arctic Ocean sea ice cover: 370 Reconstruction from biomarkers, Paleoceanography, 30, doi:10.1002/2015PA002814, 2015.

375

380

Depth (m)	Lab ID	^{14}C Age (years BP)	Error (years)	Calibrated median age (years BP)	Assigned prior uncertainty range (years)	Note/Material
0	–	–	–	–	0-400	Surface tie point
1.4	OS-134758	8910	±40	9262	8289-10236	Mollusk shell
2.505	OS-137059	16100	±120	19421	8289-19574	Bulk
3.905	OS-134522	17450	±130	21077	8289-21275	Bulk
4.305	OS-136332	20600	±150	24808	8289-25040	Bulk
4.705	OS-134523	16900	±130	20381	8289-20549	Bulk
5.805	OS-134524	22900	±270	27195	8289-27505	Bulk
6.405	OS-136336	36400	±1100	40821	20821-41905	Bulk
7.275	OS-144758	27900	±450	31850	11850-32298	Bulk
7.675	OS-134525	29500	±640	33541	13541-34238	Bulk

Table 1: Chronological information for core SWR-31PC used to construct the chronology presented in this study and shown in Figure 3. To account for an unknown local reservoir age during the early Holocene, the mollusk shell age was calibrated using a correction of $\Delta R = 0^{+1000}_{-400}$. Prior uncertainty range of bulk ages was calculated using their maximum calibrated age, and their median calibrated age minus 20,000 years to conservatively account for an unknown amount of ^{14}C-dead carbon. If the calibrated bulk age minus 20,000 years is younger than the minimum calibrated age of the marine mollusk, the latter is assigned as lower age boundary.
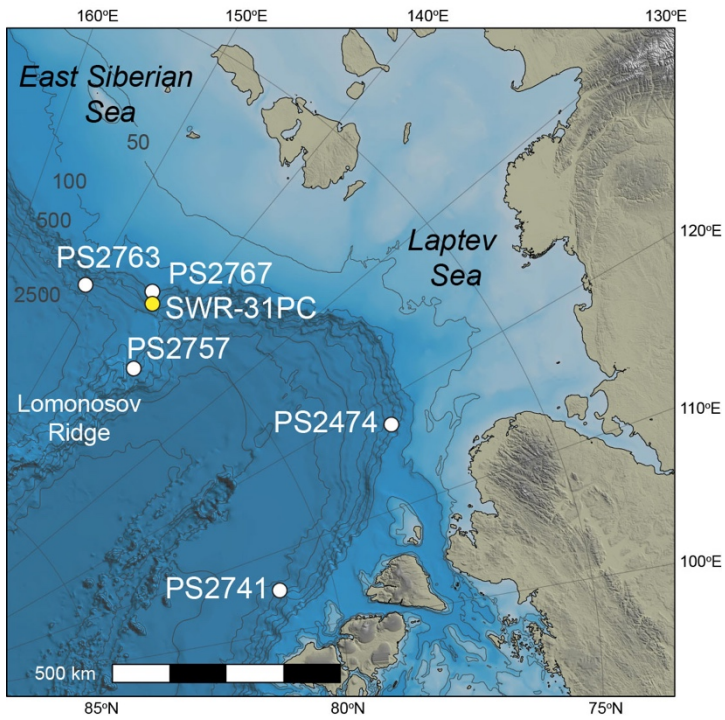
410   **Figure 1: Map of study area with location of core SWR-31PC and regional sites used in the construction of the pre Holocene and postglacial sediments of PS2767 by (Stein et al., 2001).**
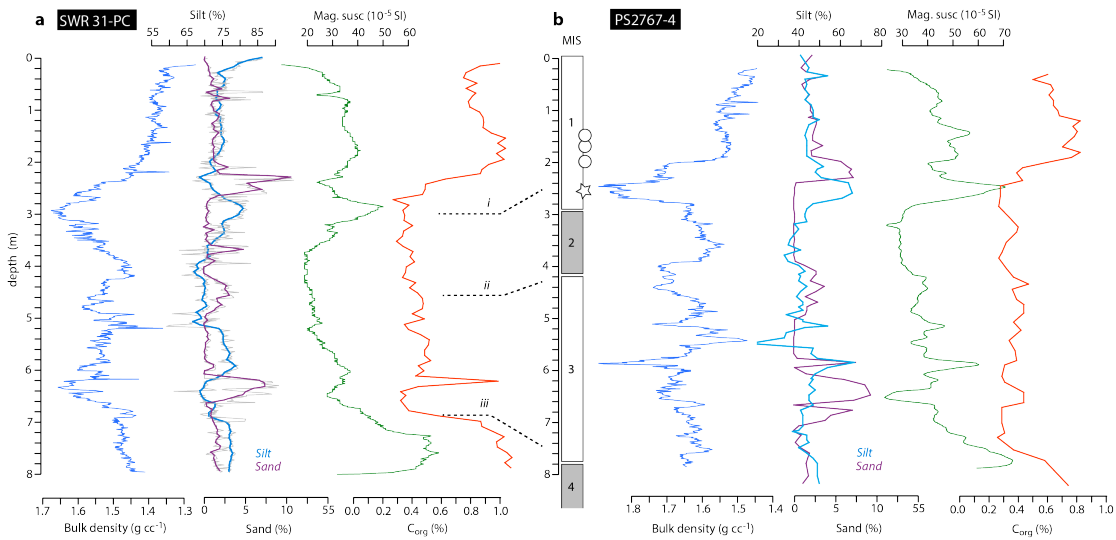
Figure 2: a-b. Lithostratigraphy of cores SWR-31-PC and PS2767-4 based on physical property measurements. The overall
415 **similarity in the sedimentary sequences is clear, and illustrated using three prominent horizons: *i*) A pronounced peak in magnetic susceptibility that accompanies a notable reduction in the silt and subsequent increase in the sand fraction. This interval precedes a clear increase in the organic carbon content of both records. *ii*) A 40-60 cm silt and sand enriched layer that is also captured in the higher resolution bulk density records from each core, and *iii*) An interval of increased magnetic susceptibility and organic carbon content that extends from the base of each core, and ends before a prominent correlative**
420 **peak in the sand content. The Marine Isotope Stage boundaries (after (Lisiecki and Raymo, 2005)) proposed by (Fahl and Stein, 2012) for PS2767-4 are shown. Circles are direct radiocarbon dates on mollusk shells in PS2767-4 (Müller and Stein, 2000) while the star marks the correlated placement of a radiocarbon date obtained from a mollusk shell in PS2741 (Stein et al., 2001).**
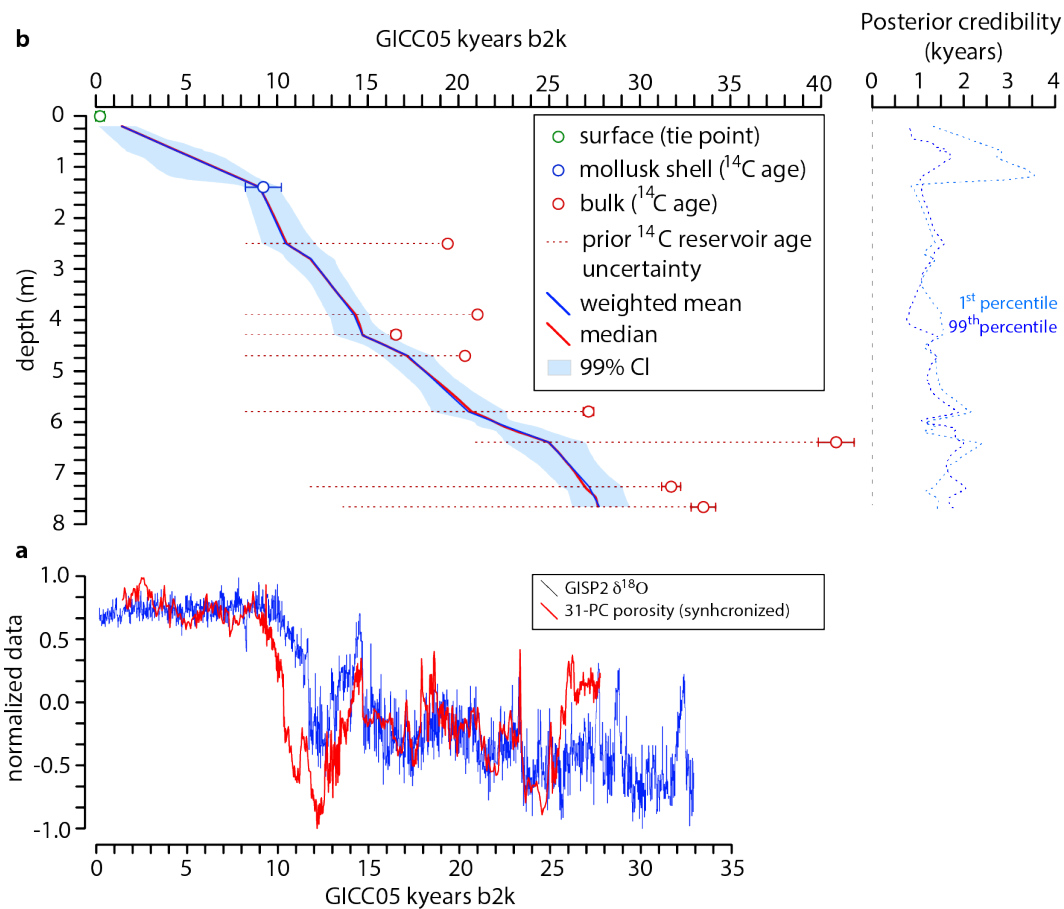
Figure 3: a. Weighted mean placement of SWR-31PC porosity record on the GICC05 timescale (Rasmussen et al., 2006) via correlation to GISP2 δ^{18}O data. The records are presented in normalized units. b. Probabilistic age model of SWR-31PC based on ^{14}C age constraints and stratigraphic alignment to GISP2 δ^{18}O. Solid bars reflect age range of calibrated ages. Dashed lines show the maximum age uncertainty range assigned to each date to inform the MCMC alignment model. Posterior 99% credible intervals of the alignment relative to the weighted mean age estimate are shown in the right-hand panel.
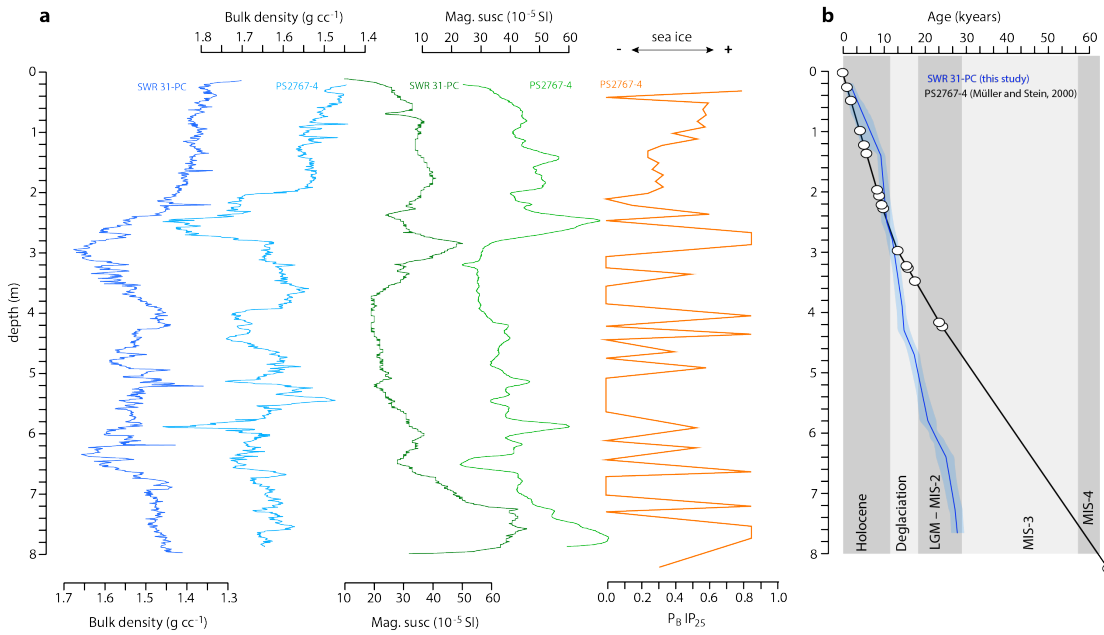
Figure 4: a. Profiles of sedimentological/geochemical properties of core SWR-31PC (this study) and core PS2767-4 (Müller and Stein, 2000) on their independent depth scales. A semi-quantitative reconstruction of sea-ice conditions from core PS2767-4 based on the brassicasterol- IP$_{25}$ index (P$_B$IP$_{25}$) is also presented (Xiao et al., 2015). b. Age-depth model comparison between core SWR-31PC and PS2767-4. Blue shading reflect the 99% confidence limit of the age model of core SWR-31PC. White dots reflect tie points/age constraints used to construct the chronology of core PS2767-4 (Müller and Stein, 2000). Note stratigraphic similarities between the sedimentological signals as opposed to the large age offset prior to ~14 kyr BP.